

# ACCRETION ONTO THE COMPANION OF ETA CARINAE DURING THE SPECTROSCOPIC EVENT. IV. THE DISAPPEARANCE OF HIGHLY IONIZED LINES

Noam Soker<sup>1</sup>

## ABSTRACT

We show that the rapid and large decrease in the intensity of high-ionization emission lines from the  $\eta$  Carinae massive binary system can be explained by the accretion model. These emission lines are emitted by material in the nebula around the binary system that is being ionized by radiation from the hot secondary star. The emission lines suffer three months long deep fading every 5.54 year, assumed to be the orbital period of the binary system. In the accretion model, for  $\sim 70$  day the less massive secondary star is accreting mass from the primary wind instead of blowing its fast wind. The accretion event has two effects that substantially reduce the high-energy ionizing radiation flux from the secondary star. (1) The accreted mass absorbs a larger fraction of the ionizing flux. (2) The accreted mass forms a temporarily blanketed around the secondary star that increases its effective radius, hence lowering its effective temperature and the flux of high energy photons. This explanation is compatible with the fading of the emission lines at the same time the X-ray is declining to its minimum, and with the fading being less pronounced in the polar directions.

*Subject headings:* (stars:) binaries: general—stars: mass loss—stars: winds, outflows—stars: individual ( $\eta$  Carinae)

## 1. INTRODUCTION

The two winds blown by the massive stellar binary system  $\eta$  Car are major players in the 5.54 yr light periodicity. The periodic variation is observed from the IR (e.g., Whitelock et al. 2004) to the X-ray band (Corcoran 2005; Corcoran et al. 2001, 2004a,b). According to most models, the periodic winds interaction behavior follows the 5.54 years periodic change

---

<sup>1</sup>Department of Physics, Technion—Israel Institute of Technology, Haifa 32000 Israel; soker@physics.technion.ac.il.

in the orbital separation in this highly eccentric,  $e \simeq 0.9$ , binary system (e.g., Hillier et al. 2006). The X-ray deep minimum lasts  $\sim 70$  day and occurs more or less simultaneously with the spectroscopic event (e.g., Damineli et al. 2000), defined by the fading, or even disappearance, of high-ionization emission lines (e.g., Fe III  $\lambda 1895$ , Fe III  $\lambda 4701$ , Ne III  $\lambda 1747-54$ , Si III  $\lambda 1892$ , Zanella et al. 1984; He I  $\lambda 10830$ , Damineli 1996; He I  $\lambda 6678$ , Damineli et al. 2000; and many more lines listed by Damineli et al. 1998). The spectroscopic event includes changes in the continuum and other lines (e.g., Martin et al. 2006,a,b; Davidson et al. 2005). The X-ray minimum and spectroscopic event are assumed to occur near periastron passages.

The change in the orbital separation and absorption by the wind or a presumed eclipse by one or two of the stars cannot account for the  $\sim 70$  day long X-ray minimum (Ishibashi et al. 2003; Hamaguchi et al. 2005). To account for the deep X-ray minimum Soker (2005a,b) has suggested that for  $\sim 10$  weeks near periastron passages the secondary does accrete mass from the primary wind. The collision region of the two winds, a very fast wind from the secondary star and a slower wind from the primary star, is responsible for the X-ray emission along most of the orbit (Corcoran et al. 2001; and Pittard & Corcoran 2002; Akashi et al. 2006). According to the accretion model the deep minimum is assumed to result from the collapse of the collision region of the two winds onto the secondary star. This process is assumed to shut down the secondary wind, hence the main X-ray source. Akashi et al. (2006) showed that this assumption provides a phenomenological description of the X-ray behavior around the minimum. The accretion model was applied also (Soker & Behar 2006) to explain the appearance of the He II  $\lambda 4686$  emission line before the event and its disappearance during the event (Steiner & Damineli 2004; Martin et al. 2006b).

One of the motivations for developing the accretion model for the spectroscopic event is the problem of the single star shell-ejection model (Zanella et al. 1984) to account for the X-ray decline (Akashi et al. 2006). Hamaguchi et al. (2005) observed  $\eta$  Car 24 days into the minimum (on 2003-07-22) with XMM-Newton. Despite the huge decline, the X-ray spectrum does not become harder, as would be expected if absorption is responsible for the decline in X-ray intensity. This shows that absorption cannot be the main reason for the X-ray decline. After another several days the X-ray luminosity starts to increase for a while (Corcoran 2005), and becomes harder (Corcoran 2005; Hamaguchi et al. 2005). This again contradicts an absorption effect in which a rise in flux (less absorption) would be accompanied by softening. In addition, in the shell ejection model the stellar primary mass loss rate should increase by a factor of  $\sim 20$  (Corcoran et al. 2001). There is a larger question regarding the mechanism capable of increasing the mass loss rate by this large factor (Soker 2005a). In any case, an increase by a factor of  $\sim 20$  in the primary mass loss rate in the equatorial plane will make accretion onto the secondary inevitable. Even without this increase accretion is suggested to occur in the accretion model. Therefore, any model for a

periastron increase in primary mass loss rate must consider accretion onto the companion. In addition, in a recent paper Nielsen et al. (2007) interpret their spectroscopic data as strong support for binarity over a single star shell-ejection.

The accretion process might lead to the formation of an accretion disk for a very short time (Soker 2003, 2005a), and might even lead to a transient launching of two opposite jets, as suggested theoretically (Soker 2005a; Akashi et al. 2006), and might have been observed (Behar et al. 2006). Basically, in a steady state Bondi-Hoyle type accretion flow (see below) the accreted mass has not enough angular momentum to form an accretion disk. However, stochastically accreted blobs at the onset of the accretion phase might lead to the formation of a transient accretion disk, and possibly to two jets. Earlier suggestions for a disk in  $\eta$  Car were made by van Genderen et al. (1994, 1999). The accretion process proposed to occur for only  $\sim 10$  weeks near periastron passage in present  $\eta$  Car is different from what was presumably happening during the Great Eruption. The Great Eruption (Davidson & Humphreys 1997) is the 20 years event that led to the formation of the bipolar nebulae around  $\eta$  Car (the Homunculus) starting one hundred and seventy years ago.

Few words on the accretion process are in place here. The accretion flow structure is of a compact object of mass  $M_2$ , the secondary star, moving with a speed  $v_1$  through a cloud, the primary wind. This case was studied by Bondi & Hoyle (1944). The gas flows toward the compact object and pass through a shock wave. When the gas radiative cooling time is very short, as is the case here, the shock wave bends backward, and most of the mass is accreted from a region behind the star, called the accretion column (see fig. 1). For the present model, this implies that during the accretion process the secondary ionizing radiation will also be blocked to directions opposite the primary direction. The gas that is accreted is the gas that flows within a distance of  $< R_{acc2}$  from the accreting object. Here  $R_{acc2}$  is the accretion radius, which is more or less the Bondi-Hoyle accretion radius  $R_{acc2} \simeq 2GM_2/v_1^2$ .

For the typical parameters of  $\eta$  Car, the accretion radius is always much smaller than the orbital separation,  $R_{acc2} \lesssim 0.2r$  (Soker 2005b; Akashi et al. 2006). Therefore, the latitude dependence of the primary mass loss rate and velocity (Smith et al. 2003) is not significant for the model. What is important is the primary wind portion that interacts with the secondary wind. This is the portion that is blown near the equatorial plane, and its properties are determined from the X-ray emission (Pittard & Corcoran 2002; Akashi et al. 2006).

For the accretion process to take place, the primary wind should reach a distance of  $\lesssim R_{acc2}$  from the secondary. For most of the orbit the secondary wind prevents the primary wind to reach this distance (Soker 2005b; Akashi et al. 2006). However, near periastron passages the colliding region of the two winds gets closer to the secondary star, and accretion

is likely to take place (Soker 2005b). A higher mass loss rate from the primary will push the colliding region closer to the secondary, hence will make the accretion process more pronounced.

The initiation of the  $\sim 10$  weeks accretion phase was discussed in Soker (2005b). Until 3D numerical gas-dynamical simulations are performed, the initiation processes of the accretion phase outlined below should be considered as a scenario, rather than an established model. Because of thermal instabilities dense large blobs are formed in the post-shock primary's wind region near the stagnation point. As periastron is approached the colliding wind region near the stagnation point gets closer to the secondary star, the secondary's gravity influence on these blobs increases, and just prior to periastron passage the blobs become bound to the secondary's, and fall onto it. Very close, possibly  $\sim 10$  day prior, to periastron passage the mass of the primary's wind that is accreted is assumed to be large enough to shut down the secondary wind. The assumed shut-down must be a non-linear process, because the mass accretion rate is smaller than the mass loss rate of the secondary. As the secondary's wind no longer reaches the previous stagnation region, the primary wind flows toward the secondary and the Bondi-Hoyle type accretion flow starts. A key assumption in the model is that blobs accreted near periastron passage shut down, or substantially weaken, the secondary wind. After  $\sim 10$  weeks the orbital separation substantially increases such that the mass accretion rate declines and the secondary wind rebuilds itself.

In the present paper we try to explain the fading and disappearance of high-ionization emission lines, from the near UV to the near IR, with the accretion model (Soker 2005b). This is a 4th paper in a series of papers aiming at understanding the spectroscopic event by an accretion process onto the secondary star during the event. The reader should consult earlier papers for more details on the accretion process.

## 2. THE BINARY SYSTEM

The  $\eta$  Car binary parameters used by us are as in the previous papers in this series (Soker 2005b; Akashi et al. 2006; Soker & Behar 2006). They are based on several papers and taking into account the present disagreement on some of the binary parameters (e.g., Ishibashi et al. 1999; Daminieli et al. 2000; Corcoran et al. 2001, 2004b; Hillier et al. 2001; Pittard & Corcoran 2002; Smith et al. 2004). The assumed stellar masses are  $M_1 = 120M_\odot$ ,  $M_2 = 30M_\odot$ , the eccentricity is  $e = 0.9$ , and orbital period 2024 days, hence the semi-major axis is  $a = 16.64$  AU, and the orbital separation at periastron is  $r = 1.66$  AU. The mass loss rates are  $\dot{M}_1 = 3 \times 10^{-4}M_\odot \text{ yr}^{-1}$  and  $\dot{M}_2 = 10^{-5}M_\odot \text{ yr}^{-1}$ . The terminal wind speeds are taken to be  $v_1 = 500 \text{ km s}^{-1}$  and  $v_2 = 3000 \text{ km s}^{-1}$ . It is assumed here, and in the previous

papers in the series, that the orbital plane is oriented in the same plane as the equatorial zone of the primary’s wind, and the equatorial plane of the Homunculus.

The secondary can be assumed to be an O star. Somewhat evolved main sequence O-stars with  $M_2 = 30M_\odot$  can have an effective temperature of  $T_2 \simeq 40,000$  K, and a luminosity of  $L_2 \simeq 3 \times 10^5 L_\odot$ , hence a radius of  $R_2 \simeq 11R_\odot$ ; such stars have mass loss rates of up to  $\sim 10^{-5}M_\odot \text{ yr}^{-1}$  (e.g., Repolust et al. 2004). These estimates are associated with large uncertainties since most likely the secondary underwent a massive accretion event during the Great Eruption (Soker 2001, 2004, 2007), which ended  $\sim 150$  yr ago and hence it is likely to be out of thermal equilibrium. Recently, Verner et al. (2005) deduced the following secondary properties:  $T_2 \simeq 37,200$  K,  $L_2 \simeq 9.3 \times 10^5 L_\odot$ ,  $R_2 \simeq 23.6R_\odot$ ,  $v_2 = 2000 \text{ km s}^{-1}$ , and  $\dot{M}_2 \simeq 8.5 \times 10^{-6}M_\odot \text{ yr}^{-1}$ . We follow Soker & Behar (2006) and take  $R_2 = 20R_\odot$  and  $T_2 = 40,000$  K. The primary star is more luminous but it is larger, and its effective temperature is much lower. Therefore, it is the secondary star that ionizes the gas that is the source of the high-ionization emission lines (Verner et al. 2005).

To demonstrate the crucial role of the accretion of primary’s wind by the secondary star we examine the ionizing flux at two energies, corresponding to ionization of hydrogen and helium. The rate of ionizing photons per steradian, i.e., having energy of  $h\nu > 13.6$  eV to ionize hydrogen and  $h\nu > 24.6$  eV to ionize helium, emitted by the secondary star depends on its temperature. The dependance of the ratio of ionizing photons to stellar luminosity on effective temperature (Schaerer & de Koter 1997) can be fitted with a linear relation for both helium and hydrogen ionizing photons in the range  $35,000 \lesssim T_2 \lesssim 42,000$  K. The number of photons emitted per stellar energy output is given by

$$\begin{aligned} n(h\nu > 13.6 \text{ eV}) &= \left( 43 \frac{T_2}{40,000 \text{ K}} - 30.4 \right) \times 10^9 \text{ photon erg}^{-1} & 30,000 \lesssim T_2 \lesssim 42,000 \\ n(h\nu > 24.6 \text{ eV}) &= \left( 23 \frac{T_2}{40,000 \text{ K}} - 20 \right) \times 10^9 \text{ photon erg}^{-1} & 35,500 \lesssim T_2 \lesssim 42,000 \end{aligned} \quad (1)$$

We here give the ionizing photon rate at two temperatures which we consider the bounds of reasonable values for the secondary in  $\eta$  Car; a linear fit can be done for any effective temperature in the above range.

$$\dot{N}_{i2} = \frac{\dot{N}_{i2-t}}{4\pi} = \frac{L_2}{9 \times 10^5 L_\odot} \text{ s}^{-1} \text{ sr}^{-1} \begin{cases} 3.5 \times 10^{48} & \text{Hydrogen } T_2 = 40,000 \text{ K} \\ 2.3 \times 10^{48} & \text{Hydrogen } T_2 = 36,000 \text{ K} \\ 8.2 \times 10^{47} & \text{Helium } T_2 = 40,000 \text{ K} \\ 1.9 \times 10^{47} & \text{Helium } T_2 = 36,000 \text{ K} \end{cases} \quad (2)$$

### 3. THE IONIZING RADIATION PROPAGATION THROUGH THE WIND

#### 3.1. The Undisturbed Primary Wind

Let us consider the distance to which the secondary ionizes the undisturbed primary wind along a direction perpendicular to the orbital plane. By undisturbed we mean that the influence of the secondary gravity and wind on the primary wind is neglected. The density of the secondary wind is very low, and it can be neglected when calculating the recombination rate. The density of the undisturbed primary wind as function of distance  $y$  perpendicular to the orbital plane measured from the secondary is  $\rho_1(y) = \dot{M}_1/4\pi(r^2 + y^2)v_1$ , where  $r$  is the orbital separation. The total hydrogen recombination rate per steradian along that direction is

$$\dot{R}_{\text{pole}} = \alpha_B \int_0^\infty n_e n_H y^2 dy = 0.22\alpha_B \left( \frac{\dot{M}_1}{4\pi v_1 \mu m_H} \right)^2 \int_0^\infty \frac{y^2}{(r^2 + y^2)^2} dy, \quad (3)$$

where  $\alpha_B$  is the recombination coefficient and  $\mu m_H$  is the mean mass per particle in a fully ionized gas. A similar expression can be derived for the recombination rate of  $He^+$ , assuming that its abundance by number is 10%. Performing the integral and substituting typical values gives for the recombination rate per steradian

$$\dot{R}_{\text{pole}} = \left( \frac{\dot{M}_1}{3 \times 10^{-4} M_\odot \text{ yr}^{-1}} \right)^2 \left( \frac{v_1}{500} \right)^{-2} \left( \frac{r}{5 \text{ AU}} \right)^{-1} \text{ s}^{-1} \text{ sr}^{-1} \begin{cases} 5.4 \times 10^{47} & \text{Hydrogen} \\ 5.7 \times 10^{46} & \text{Helium.} \end{cases} \quad (4)$$

The orbital separation of 5 AU is the one at  $\sim 35$  day before and after periastron. In deriving equation (4) we assumed a spherical mass loss geometry and ignored the dependence of the primary wind's density and velocity on latitude (Smith et al. 2003).

Along a direction from the secondary to the opposite side of the primary (right side in Figure 1), the recombination rate through the undisturbed primary wind,  $\dot{R}_b$ , is obtained by replacing  $(r^2 + y^2)^2$  with  $(r + y)^4$  in the denominator of equation (3); the recombination rate is smaller by a factor of  $3\pi/4$

$$\left( \frac{\dot{R}_b}{\dot{R}_{\text{pole}}} \right)_0 = \frac{4}{3\pi} = 0.42, \quad (5)$$

where subscript zero indicates that this expression holds for the undisturbed primary wind.

Comparing equations (4) and (5) with equation (2) teaches us that the secondary can (for the chosen parameters) ionize the undisturbed primary wind to large distances along the polar directions and the equatorial directions away from the primary. The recombination rate is quite sensitive to the primary wind's properties. An increase by a factor of  $\sim 3$  in

the ratio  $\dot{M}_1/v_1$  (namely, an increase in the mass loss rate and/or a decrease in the wind speed) will result in an ionization distance through the undisturbed primary wind smaller than the distance to the regions that emit the emission lines, e.g., the Weigelt blobs, when  $r = 5$  AU. For a mass loss rate as high as  $\dot{M}_1 \gtrsim 3 \times 10^{-3} M_\odot \text{ yr}^{-1}$  the Strömgren radius is within the wind at all orbital separations even for the undisturbed primary wind. Martin et al. (2006c) suggested that at the beginning of the 20th century the primary stellar mass loss rate was much higher,  $\dot{M}_1 \sim 10^{-2} M_\odot \text{ yr}^{-1}$ , such that many emission lines were not observed at all. We instead suggest that the secondary was cooler, hence had weaker ionizing radiation (section 5).

### 3.2. The Shocked Primary Wind

The secondary wind ‘cleans’ the area behind the secondary (right side in Figure 1) and compresses the primary wind along the contact discontinuity, increasing the recombination rate there. Therefore, the ratio between the recombination rate in the equatorial plane in the direction away from the primary,  $\dot{R}_b$ , and that in the polar directions,  $R_{\text{pole}}$ , is much smaller than the value given by equation (5) for the undisturbed primary wind. The half opening angle of the wind-collision cone (see Figure 1) is  $\phi_a \simeq 60^\circ$  (Akashi et al. 2006). This implies that even as the secondary approaches or recedes periastron the secondary fast wind will clean a large solid angle for ionization to propagate almost unattenuated at low latitudes, unless the fast wind is shut down as assumed here (see section 3.3).

The post-shock primary wind has a much higher density and hence its high recombination rate must be considered. The postshock region is unstable, and has a corrugated structure (Pittard & Corcoran 2002; Pittard et al. 1998). For that, our calculation here is a crude estimate, but still teaches us on the importance of the shock wave. The post-shocked primary wind flows in a thin shell along the contact discontinuity. Let the width of the conical shell along the polar direction at distance  $y_p$  from the secondary be  $d_p$ ; these quantities are defined in Figure 1. The primary wind rapidly cools to a temperature of  $T_p \simeq 10^4$  K, and it is compressed by the ram pressure of the slow wind to a density  $\rho_p$ . Neglecting first the magnetic pressure in the post-shock region,  $\rho_p$  is given by equating the thermal pressure  $kT_p\rho_p/\mu m_H$  of the post-shock material with the ram pressure of the primary wind  $\rho_1(v_{\text{wind1}} \sin \beta)^2$ , where  $\beta$  is the angle between the slow wind speed and the shock front at  $y_p$ , and  $v_{\text{wind1}}$  is the pre-shock speed of the primary wind relative to the stagnation point. For the present purpose we can take  $v_{\text{wind1}} \simeq v_1$ . From Figure 2 of Pittard & Corcoran (2002) we find  $\beta(y_p) \sim 30^\circ$  and  $y_p \sim 0.5 - 0.6r$ . For a post-shock temperature of  $T_p \simeq 10^4$  K we

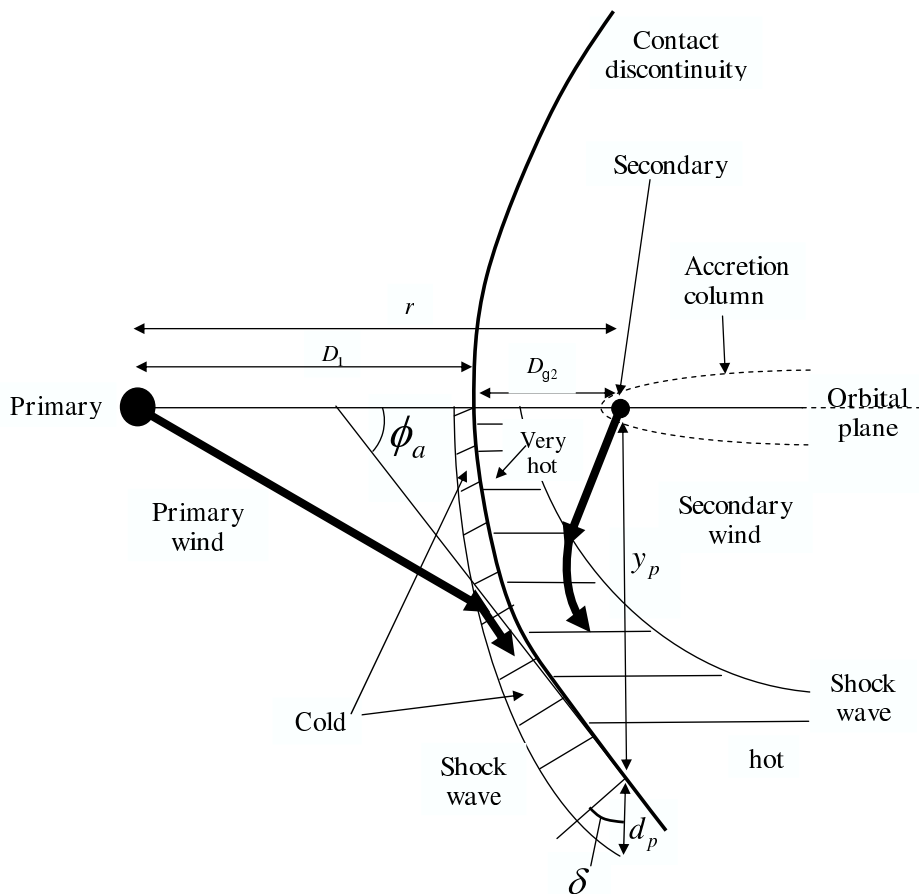


Fig. 1.— Schematic drawing of the collision region of the two stellar winds and definition of several quantities. The two thick lines represent winds’ stream lines. The two shock waves are drawn only in the lower half. The post-shock regions of the two winds are hatched. The dashed line shows the accretion column which exists, according to the proposed model, only for  $\sim 70 - 80$  days during the accretion period which corresponds to the X-ray minimum and the spectroscopic event (adopted from Akashi et al. 2006).

find

$$\left(\frac{\rho_p}{\rho_1}\right)_{\text{thermal}} \simeq 470 \left(\frac{v_1}{500 \text{ km s}^{-1}}\right)^2 \left(\frac{\sin \beta}{0.5}\right)^2. \quad (6)$$

Such a high density contrast is seen in Figure 2 of Pittard & Corcoran (2002). However, because of magnetic fields we don't expect such a large compression behind the shock. Typical pre-shock magnetic pressure to ram pressure ratio can be  $\eta_B \equiv P_{B0}/\rho_1 v_1^2 \sim 0.001 - 0.1$  (e.g., Eichler & Usov 1993; Pittard & Dougherty 2006). The magnetic field component parallel to the shock is increased as it is compressed when the density is increased in the shock wave. For a random field we can take this component to contribute 1/3 to the pre-shock pressure. Equating the post-shock magnetic pressure to the wind's ram pressure we find the limit on the compression factor imposed by the magnetic field to be

$$\left(\frac{\rho_p}{\rho_1}\right)_B \simeq \left(\frac{3}{\eta_B}\right)^{1/2} \simeq 30 \left(\frac{\eta_B}{0.003}\right)^{-1/2}. \quad (7)$$

More than that, the strong magnetic field can smooth the strong corrugated structure seen in the simulations presented by Pittard & Corcoran (2002). The presence of the magnetic field is another source of the large uncertainties involved in our calculation, and it can introduce large stochastic variations on short time scale and from cycle to cycle. Considering equations (6) and (7) we will use the scaling  $\rho_p/\rho_1 = 100$ .

If the post-shock gas outflows at a speed  $v_d$  along the contact discontinuity, then mass conservation for the mass entering the region  $y \leq y_p$  reads

$$\dot{M}_1(y_p) \equiv \frac{1}{2} \left[ 1 - \frac{r}{(r^2 + y_p^2)^{1/2}} \right] \dot{M}_1 \simeq 2\pi v_d \rho_p y_p d_p \cos \delta, \quad (8)$$

where the angle  $\delta$  is defined in Figure 1. The velocity  $v_d$  of the post-shock primary wind parallel to the shock front is zero at the stagnation point (where the two winds momenta balance each other along the symmetry axis), and increases to  $\sim v_1$  at infinity. Mixing between the two winds, as a result of instability (the corrugated structure; Pittard & Corcoran 2002), will further accelerate the post-shock primary wind (Girard & Willson 1987). This happens because the post-shock secondary wind expands faster than the primary wind and because of its long cooling time it has a pressure gradient parallel to the contact discontinuity. We therefore can take  $0.5v_1/v_d \cos \delta \sim 1$ . Substituting typical values in equation (8) gives

$$\frac{d_p}{y_p} \simeq \frac{v_1}{v_d} \frac{0.5}{\cos \delta} \frac{\rho_1}{\rho_p} \simeq \frac{\rho_1}{\rho_p}. \quad (9)$$

The recombination rate per steradian for the undisturbed wind up to distance  $y = y_p$  from the secondary goes as  $\dot{R}_0(y_p) \simeq \alpha_B n_e n_p y_p^3/3 \propto y_p^3 \rho_1^2/3$ , while in the post-shock

shell at  $y = y_p$  it is  $\dot{R}_{\text{shock-pole}}(y_p) \simeq \alpha_B n_e n_p y_p^2 d_p \propto y_p^2 d_p \rho_p^2$ . Using equation (9) we find  $\dot{R}_{\text{shock-pole}}(y_p) \simeq 3(\rho_p/\rho_1)\dot{R}_0(y_p)$ . We find that the recombination rate in the postshock region is much higher than that in the undisturbed slow wind occupying the same region. Substituting typical values that we used above, with  $y_p = 0.55r$ , we find the recombination rate per steradian of the shocked gas

$$\dot{R}_{\text{shock-pole}}(y_p) \simeq \left( \frac{\dot{M}_1}{3 \times 10^{-4} M_\odot \text{ yr}^{-1}} \right)^2 \left( \frac{v_1}{500} \right)^{-2} \left( \frac{r}{5 \text{ AU}} \right)^{-1} \frac{\rho_p}{100\rho_1} \text{ s}^{-1} \text{ sr}^{-1} \begin{cases} 10^{49} & \text{Hydrogen} \\ 10^{48} & \text{Helium.} \end{cases} \quad (10)$$

Comparing equation (10) with equation (2) shows that for an orbital separation of  $r \simeq 5 \text{ AU}$  the recombination rate along the polar directions is about equal to the ionization rate. This implies that the ionization structure of the primary wind will change as the two stars orbit each other, and that this structure is sensitive to the primary wind properties: mass loss rate, speed, magnetic field. This sensitivity can result in stochastic variation from cycle to cycle and within one cycle. The primary wind parameters, and in particular the compression ratio within the shock can be constraint from the free-free radio emission of  $\eta \text{ Car}$ . This will be the subject of a forthcoming paper.

### 3.3. The Path Opened by the Secondary Wind

The derivation of subsections (3.1) and (3.2) is true for directions through the primary wind. The secondary wind opens a large solid angle through which the secondary ionizing radiation can freely expand to infinity. For example, the radiation can reach the Weigelt blobs from where high-ionization emission lines are observed (Hamann et al. 2005; Hartman et al. 2005; Johansson et al. 2006). This is shown before and after periastron passage in Figure 2. This solid angle is to a side opposing the primary wind (the right side of the secondary star in Figure 1), and the asymptotic opening angle of this region is  $\phi_a \simeq 60^\circ$  (Akashi et al. 2006). Therefore, if the secondary continues to blow its wind during the spectroscopic event a large fraction of the ionizing radiation will reach far regions in the equatorial plane even when the binary system is near periastron, and there will be no large fading in high ionization emission lines. The decrease in orbital separation can account for a slower variation, like the slow decline in the  $H_\alpha$  which starts 3 months before the event (Davidson et al. 2005). Three months before periastron passage the orbital separation is  $\sim 10 \text{ AU}$ , and a reduction in the ionizing photons reaching large distance can be significant (depending on the exact primary wind's parameters).

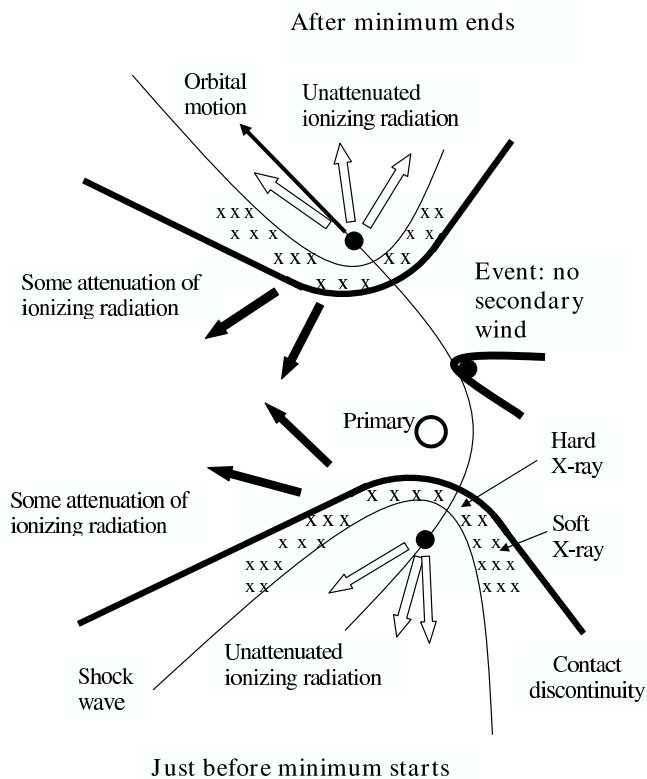


Fig. 2.— Schematic drawing (not for scaling and not the exact shock waves and contact discontinuity structures) of the flow structure at three epochs: Just before and after the spectroscopic event, or the X-ray minimum, when the two winds exist, and during the X-ray minimum, when the secondary wind is assumed to be extinct. Note that according to our model the X-ray minimum and the spectroscopic event are not symmetric about periastron. The shocked primary wind is marked by the thick arcs; the X-ray emitting shocked secondary wind is in the region marked by ‘x’s’; the open and filled circles mark the positions of the primary and secondary, respectively. Secondary stellar ionizing radiation escaping through the secondary wind suffers almost no attenuation (empty arrows). During the event, the accretion column absorbs the radiation along that direction, while the dense primary wind absorbed the radiation in the primary direction. Hence, no hard ionizing radiation escape in the equatorial plane during the event (adopted from Akashi et al. 2006).

The general flow structure and ionization and recombination rates we deal with are far too sensitive to the stellar and wind parameters to be modelled by a simple approach. However, some estimates can be done. The primary is too cool to ionize helium at large distances and in all directions, so the much hotter secondary must be the source of the harder ionizing radiation (e.g., Steiner & Damiani 2004; Verner et al. 2005). Davidson & Smith (2006) argued for a hot primary’s equatorial photosphere,  $> 20,000$  K. In the past it was argued that most of the photons with energy  $h\nu > 13.6$  eV emitted by the primary are absorbed by the wind (Davidson & Humphreys 1997; Hillier et al. 2001). Hillier et al. (2001) found that the hydrogen in the wind becomes neutral at a distance of  $\sim 200$  AU from the star. They used a high mass loss rate of  $\dot{M}_1 = 10^{-3}M_\odot \text{ yr}^{-1}$ , and small filling factor for the wind (large clumping), and may have overestimated the global recombination rate in the wind. Smith et al. (2003) found the stellar wind in the polar directions to be denser than the wind blown at low latitudes and the equatorial direction. The strong absorption seen in Balmer lines toward high latitudes indicate that there is a large fraction of neutral hydrogen there. Smith et al. (2003) argued that in the equatorial plane the wind might be largely ionized, hence allowing the primary radiation to reach the Wigelt blobs. The decrease in many emission lines with no decrease in the visual continuum (Martin & Koppelman 2004) suggests that the cause of the spectroscopic event is in the secondary star, and not in the much brighter primary star.

Najarro et al. (1997) studied the ionization structure of the wind from P Cygni and found that the wind ionization structure as a result of the ionizing radiation of the star blowing the wind is both complicated and sensitive to the stellar parameters. Although, our simple approach cannot be used to deduce the exact ionizing effect of the primary radiation, as discussed above, we can do a simple estimate. For the parameters used here the number of hydrogen-ionizing photons emitted by the secondary is  $\sim 3$  times larger than that from the primary star (say for  $R_1 = 120R_\odot$  and  $T_{\text{eff}1} = 25,000$  K). The recombination rate along a line from the star is proportional to  $1/r_{\text{min}}$ , where  $r_{\text{min}}$  is the radius where the absorption starts. The primary radius is  $< 0.6$  AU, and therefore the recombination rate from the primary to large distances is  $\sim 10$  times larger than that from the secondary when the secondary is at an orbital separation of 5 AU, the distance that was used in sections (3.1) and (3.2). Because of the primary wind-acceleration zone, where wind density is higher, the recombination rate along a ray from the primary will be larger even. With the primary ionization rate lower by a factor of  $\sim 3$  and recombination rate along a ray larger by a factor of  $> 10$ , compared with the secondary, and using numbers we derived in equations (2), (4) and (10), we conclude that ionization by the primary is less important than that by the secondary star. Considering all these and the results of Verner et al. (2005), we concentrate on ionization by the secondary star and the influence of the accretion flow near periastron passages on the ionization process.

#### 4. THE IONIZATION DURING THE ACCRETION PHASE

There are several arguments why the spectroscopic event cannot be a simple eclipsing event or a burial of the secondary inside the primary wind (Stahl et al. 2005). For example, in all directions the spectroscopic event has a fast onset and a slow recovery (Stahl et al. 2005). Such a behavior, as well as changes in emission lines intensities on time scales shorter than the time scale over which the orbital separation changes, cannot be accounted for by a simple orbital motion in an eccentric orbit. For example, a decrease by a factor of two in the intensity of some lines excited by the Lyman continuum occurs in  $\sim 3$  day (Hartman et al. 2005). This cannot be attributed to the orbital motion alone, as the fastest decrease in orbital separation occurs near periastron, and a decrease by a factor of two, for example, in orbital separation requires 18 days. We note that this behavior does not contradict the shell ejection scenario (Zanella et al. 1984). The most severe problem for the shell ejection scenario is the X-ray light curve (see section 1). The decrease in orbital separation can account for slower variations as mentioned in Sec. 3. In addition, the spectroscopic event and the X-ray minimum last  $\sim 70$  day. Even if the event is symmetric around periastron (which is probably not), the orbital separation 35 day before or after periastron is  $\sim 5$  AU, much larger than the primary radius, ruling out that the secondary is inside the primary extended atmosphere.

Instead, a change in the gas flow must occur (Zanella et al. 1984; Stahl et al. 2005; Weis et al. 2005; Davidson et al. 2005). Namely, a change in the velocity, mass loss rate, geometry of one or two of the winds blown by the two stars, and/or a change in the interaction of the two winds. We suggest that the main changes during the spectroscopic event can be attributed to an accretion event which shuts down the secondary wind (Soker 2005b). Figure 2 schematically shows the evolution around the event. According to the model (Soker 2005b; Akashi et al. 2006) during the spectroscopic event the secondary does not blow its wind, but rather accretes mass, mainly from the direction of the accretion column (the thick line attached to the secondary during the event in Figure 2; the dashed line in Figure 1).

The accretion process has two effects on the ionizing radiation emitted by the secondary. (1) *Absorption.* After the secondary wind is shut down, according to the assumption of the accretion model, and the primary wind material is accreted from the up wind direction (primary direction) and from the back through the accretion column, the large opening angle for the ionizing radiation does not exist anymore. The density along the accretion column is very large (e.g., Ishii et al. 1993; Ruffert 1996, 1999) and no ionizing radiation will escape from that direction. Now the absorption of ionizing radiation is much larger in the equatorial plane and mid-latitude directions than along the polar directions. First, the dense wind near the primary blocks the secondary radiation passing too close to the primary. Second, the

dense accretion column is in the equatorial plane. Third, as the secondary moves along its orbit the accretion column is dragged behind, and covers other directions in the equatorial plane and mid latitude (Mastrodemos & Morris 1998, 1999).

(2) *Inflated envelope.* The accreted matter has a non-negligible angular momentum. Although not enough to form an accretion disk (Akashi et al. 2006), it can still influence the accretion process. The matter will concentrate in the equatorial plane, and will take some time to reach equilibrium in the secondary’s envelope, probably several time the Keplerian orbital time,  $\tau_{\text{Kep-2}} = 1.9$  day. In addition, the secondary has a high radiation pressure on its surface, as manifest in its strong wind. This might also lengthen the relaxation time of the accreted mass onto the envelope.

During the event the Bondi-Hoyle mass accretion rate of the primary wind gas onto the secondary changes from  $\sim 0.2 \times 10^{-6} M_{\odot} \text{ yr}^{-1}$  to  $\sim 1.5 \times 10^{-6} M_{\odot} \text{ yr}^{-1}$  and then back to  $\sim 0.2 \times 10^{-6} M_{\odot} \text{ yr}^{-1}$  (Akashi et al. 2006). At the onset of accretion, as the winds collision region collapses onto the secondary, the accretion rate is higher than the Bondi-Hoyle rate. We therefore scale accretion rate with  $\dot{M}_{\text{acc}} = 10^{-6} M_{\odot} \text{ yr}^{-1}$ . We assume that this material reaches the secondary at a high speed, and encounters a shock wave. If this gas reaches the secondary at the free fall velocity of  $v_{ff2} = 760 \text{ km s}^{-1}$  (for a secondary mass of  $M_2 = 30 M_{\odot}$  and a radius of  $R_2 = 20 R_{\odot}$ ), its radiative cooling time after the shock would be  $T_{\text{cool}} \sim 2000 \text{ s}$ . The distance the flow traverse during that time is  $\sim t_{\text{cool}} v_{ff2} \simeq 2 R_{\odot}$ . Radiative breaking (Gayley et al. 1997), i.e., the radiation pressure of the secondary, will slow down the accreted mass and will increase the density calculated here.

We suggest that the accreted mass forms a blanket at a distance of a few solar radii, or  $\sim 0.1 - 0.3 R_2$ , around the secondary, and takes a few dynamical time scales to relax,  $\tau_{\text{relax}} \sim 5 \text{ day}$ ; the total mass in the blanket is  $\tau_{\text{relax}} \dot{M}_{\text{acc}}$ . The optical depth of this blanket, for an opacity of  $\kappa = 0.4$ , is

$$\tau = 0.45 \left( \frac{\dot{M}_{\text{acc}}}{10^{-6} M_{\odot} \text{ yr}^{-1}} \right) \left( \frac{t_{\text{relax}}}{5 \text{ day}} \right) \left( \frac{R_2}{20 R_{\odot}} \right)^{-2}. \quad (11)$$

The density of this material is  $\sim 10^{-11} \text{ g cm}^{-3}$ , compared with the secondary’s photospheric density of  $\rho_{\text{photosphere}} \simeq 2 \times 10^{-10} \text{ g cm}^{-3}$ .

The conclusion is that during the accretion phase the effective photosphere of the secondary star is at  $R_{p2} \sim 1.1 - 1.3 R_2$ , and its effective temperature is somewhat lower  $T_{\text{eff2}} \simeq 0.85 - 0.95 T_2$ . This can substantially reduce the energetic photon flux at  $h\nu > 24.6 \text{ eV}$ . For example, using equation (1) we find that in cooling from  $T_2 = 40,000 \text{ K}$  to  $T_{\text{eff2}} = 37,000$  (36,000) K, the ionizing flux from the secondary decreases to 0.74 (0.66) times its initial value for  $h\nu > 13.6 \text{ eV}$ , and to 0.42 (0.23) for  $h\nu > 24.6 \text{ eV}$ . If the photospheric

cooling is from  $T_2 = 38,00$  K to  $T_{\text{eff2}} = 35,500$  K, the ionizing flux from the secondary decreases to 0.74 times its initial value for  $h\nu > 13.6$  eV, and to  $\sim 0.22$  for  $h\nu > 24.6$  eV. The effect is stronger if we take  $T_2 = 37,200$  K as suggested by Verner et al. (2005). It is clear that the decrease in the flux of energetic photons,  $h\nu > 24.6$  eV, is much larger than that of lower energy photons.

Both effects, absorption and inflating the photosphere, cause more attenuation of the ionizing radiation in the equatorial plane and mid latitudes than in the polar directions. In addition, before the accretion starts there is a large opening angle formed by the low density secondary wind, through which ionizing radiation reaches large distances unattenuated. This opening solid angle is in the equatorial plane to mid-latitudes (right side in Figure 1; empty double arrows in Figure 2). Therefore, our model accounts for the observation that the spectroscopic event is more pronounced in the equatorial and mid latitudes directions than in the polar directions (Stahl et al. 2005; Weis et al. 2005). This is supported by the large changes observed in the Weigelt blobs (e.g., Hamann et al. 2005) which are thought to reside in the equatorial plane (Davidson et al. 1997). Note that if accretion does not occur during the spectroscopic event, then according to equations (5) and (10) the attenuation along the polar directions is expected to be larger than that in the back direction in the equatorial plane. This will result in larger variations along the polar directions, contrary to observations.

## 5. SUMMARY

Our goal was to explain the rapid and large decrease in the intensity of high-ionization emission lines starting with the spectroscopic event. We were not aiming at explaining the relative intensities of different lines or their exact temporal behavior, but rather to show that the accretion model can account for the basic behavior of the fading high-ionization lines. The fading of these high-ionization emission lines serves as the definition of the spectroscopic event. We appeal to the accretion model for the spectroscopic event (Soker 2005b; Akashi et al. 2006; Soker & Behar 2006). In that model some of the characteristics of  $\eta$  Car during the spectroscopic event are attributed to an accretion process where the secondary star is accreting mass from the primary wind instead of blowing its fast wind (Soker 2005b; Akashi et al. 2006; Soker & Behar 2006).

In the present papers we studied the basic behavior of the ionizing radiation emitted by the secondary star (the companion). We found that the accretion event has two effects that substantially reduce the high-energy ( $h\nu > 24.6$  eV) ionizing radiation flux that escape the vicinity of the binary system. The same effects apply, but to lesser degree, to the lower

energy photons of  $24.6 \text{ eV} > h\nu > 13.6 \text{ eV}$ .

1. *Denser circumbinary material.* Without accretion the secondary wind flows away from the binary system (to the right side in Figure 1) and ‘cleans’ a path for the secondary’s ionizing radiation to reach large distances (depicted by the empty arrows in Figure 2). In that case the attenuation expected along the equatorial plane is less than that along the polar directions (equations 5 and 10), leading to larger variations in the intensities of the high-ionization emission lines in the polar directions as the secondary orbit the primary. Observations show that the spectroscopic event is less pronounced in the polar directions than in the equatorial to mid latitude directions (Smith et al. 2003; Stahl et al. 2005; Weis et al. 2005). Therefore, the expected behavior of this model without accretion is contrary to observations. When accretion is included, larger attenuation is expected, mainly in the equatorial plane to mid latitude directions. The reason is that the accreted mass forms a dense region behind the secondary, the accretion column (dashed line in Figure 1), that has a high recombination rate, and hence prevents a large fraction of the high-energy ionizing radiation to reach large distances in and near the equatorial plane.
2. *Inflated envelope.* The accreted matter has non-negligible angular momentum (Akashi et al. 2006). The matter will concentrate in the equatorial plane, and will take some time to reach equilibrium in the secondary’s envelope, probably several times the Keplerian orbital time. In addition, the secondary has a high radiation pressure on its surface, as manifest in its strong wind. We propose that instead of an acceleration zone of the secondary wind, a blanket is formed during the accretion process, that moves the effective secondary’s photosphere to be further out. This reduces the effective temperature and the flux of high-energy photons, mainly in the equatorial plane.

These effects influence the energetic ionizing radiation, and as a result of that the behavior of high-ionization emission lines in a way compatible with observations: (i) Fading of high ionization lines at the same time the X-ray is declining to its long minimum; (ii) The fading of these lines is less pronounced in the polar directions.

The orbital motion brings the secondary into denser regions of the primary wind as it approaches periastron, and can explain relatively slow variations over the 5.54 orbital period. However, the variations due to orbital motion alone cannot account for the sharp disappearance of high-ionization emission lines during the spectroscopic event.

We emphasize that we were not aiming at explaining all complications involved in the variations of lines intensities. In particular we did not consider the following processes.

- (1) *Evolution of the primary star.* The secular variations related to the evolution of the

primary star and its wind as an LBV star (Davidson et al. 2005; Martin & Koppelman 2004; Martin et al. 2006c). We do note, however, that the evolution of the secondary can also affect the secular evolution of  $\eta$  Car. Most likely the secondary accreted several solar masses during the Great Eruption of the 19th century (Soker 2001, 2007). The accretion event  $\sim 160$  years ago drove the secondary away from equilibrium, and spun it up. It is possible that the secondary swelled, and it is contracting back since then. The contraction implies that the secondary photosphere has been heating up over the last 150 years. From angular momentum conservation we expect it to spin faster. This evolution implies that the high-energy ionization radiation flux is increasing, and the fast rotation may lead to hotter polar caps, and hence stronger ionizing radiation along the polar directions. The evolution of the secondary described above is in accord with the absence of high ionization lines before 1941 (Feast et al. 2001; Humphreys & Koppelman 2005). The secondary was larger, hence cooler, and could not ionize the region now responsible for the high-ionization emission lines. The accretion events took place before 1941, but they could not be observed via these emission lines.

Other processes not considered in the paper include:

- (2) *Density inhomogeneities in the equatorial plane.* Before the accretion phase starts radiation from the secondary is less attenuated along direction through the secondary wind (right side in Figure 11). During the orbital motion this solid angle points to different directions in the orbital plane and around it (Smith et al. (2004)). Density inhomogeneities in the equatorial plane will result in stochastic variations in line intensities.
- (3) *Variable winds.* Likewise, stochastic variation in the primary wind can lead to stochastic attenuation of the ionizing radiation.
- (4) *Non-spherical winds.* The dependence of the primary wind properties on latitude (Smith et al. 2003) were ignored in our treatment. In any case, Smith et al. (2003) find the latitude dependence of the primary wind properties to be large near apastron, whereas in the accretion the properties near periastron are important. Also, it is quite possible that this latitude dependence is influenced by the secondary star (Soker 2003).
- (5) *Collimated outflow from the secondary.* Other types of outflows suspected from the secondary star (Behar et al. 2006), that can change the ‘cleaned’ solid angle for ionizing radiation also influence the line intensities.

I thank Amit Kashi for helpful discussions, and an anonymous referee for detailed and very helpful clarifications and comments. This research was supported by a grant from the Asher Space Research Institute at the Technion.

## REFERENCES

- Akashi, M., Soker, N., & Behar, E. 2006, *ApJ*, 644, 451
- Behar, E., Nordon, R., Ben-Bassat, E., & Soker, N. 2006, (astro-ph/0606251)
- Bondi, H. & Hoyle, F. 1944, *MNRAS*, 104, 273
- Corcoran, M. F. 2005, *AJ*, 129, 2018
- Corcoran, M. F., Hamaguchi, K., Gull, T., et al. 2004a, *ApJ*, 613, 381
- Corcoran, M. F., Ishibashi, K., Swank, J. H., & Petre, R., 2001, *ApJ*, 547, 1034
- Corcoran, M. F., Pittard, J. M., Stevens, I. R., Henley, D. B., & Pollock, A. M. T. 2004b, in the Proceedings of "X-Ray and Radio Connections", Santa Fe, NM, 3-6 February, 2004 (astro-ph/0406294)
- Damineli, A. 1996, *ApJ*, 460, L49
- Damineli, A., Kaufer, A., Wolf, B., Stahl, O., Lopes, D. F., & de Araujo, F. X. 2000, *ApJ*, 528, L101
- Damineli, A., Stahl, O., Kaufer, A., Wolf, B., Quast, G., & Lopes, D. F. 1998, *A&AS*, 133, 299
- Davidson K, Ebbets D, Johansson S, Jorse J. A., Hamann F. W. 1997, *AJ*, 113, 335
- Davidson, K., Martin, J., Humphreys, R. M., Ishibashi, K., Gull, T. R., Stahl, O., Weis, K., Hillier, D. J., Damineli, A., Corcoran, M., & Hamann, F. 2005, *AJ*, 129, 900
- Davidson, K., & Humphreys, R. M. 1997, *ARA&A*, 35, 1
- Davidson, K., & Smith, N. 2006,  
[http://etacar.umn.edu/images/posters/eta\\_fuv\\_jan06.png](http://etacar.umn.edu/images/posters/eta_fuv_jan06.png)
- Eichler, D., & Usov, V. 1993, *ApJ*, 402, 271
- Feast, M., Whitelock, P., & Marang, F. 2001, *MNRAS*, 322, 741
- Gayley, K. G., Owocki, S. P., & Cranmer, S. R. 1997, *ApJ*, 475, 786
- Girard, T. & Willson, L. A. 1987, *A&A*, 183, 247
- Hamaguchi, K., Corcoran, M. F., Gull, T., White, N. E., Damineli, A., & Davidson, K. 2005, in *Massive Stars in Interacting Binaries*, preprint (astro-ph/0411271)
- Hamann, F. & The HST–Eta Carinae Treasury Team 2005, in *ASP Conf. Ser. 332*, ed R. Humphreys & K. Stanek (San Francisco: ASP), 287
- Hartman, H., Damineli, A., Johansson, S., & Letokhov, V. S. 2005, *A&A*, 436, 945
- Hillier, D. J., Davidson, K., Ishibashi, K., & Gull, T. 2001, *ApJ*, 553, 837

- Hillier, D. J., Gull, T., Nielsen, K., Sonneborn, G., Iping, R., Smith, N., Corcoran, M., Damineli, A., Hamann, F. W., Martin, J. C., & Weis, K. 2006, *ApJ*, 642, 1098
- Humphreys, R. M., & Koppelman, M. 2005, *ASPC*, 332, 159
- Ishibashi, K., Corcoran, M. F., Davidson, K., Swank, J. H., Petre, R., Drake, S. A., Damineli, A., & White, S. 1999, *ApJ*, 524, 983
- Ishibashi, K., Gull, T., Davidson, K. et al. 2003, *AJ*, 125, 3222
- Ishii, T., Matsuda, T., Shima, E., Livio, M., Anzer, U., & Boerner, G. 1993, *ApJ*, 404, 706
- Johansson, S., Hartman, H., & Letokhov, V. S. 2006, *A&A*, 452, 253
- Martin, J. C., Davidson, K., Hamann, F., Stahl, O., & Weis, K. 2006a, *PASP*, 118, 697
- Martin, J. C., Davidson, K., Humphreys, R. M., Hillier, D. J., & Ishibashi K. 2006b, *ApJ*, 640, 474
- Martin, J. C., Davidson, K., & Koppelman, M. D. 2006c, *AJ*, 132, 2717
- Martin, J. C. & Koppelman, M. D. 2004, *AJ*, 127, 2352
- Mastrodemos, N. & Morris, M. 1998, *ApJ*, 497, 303
- Mastrodemos, N. & Morris, M. 1999, *ApJ*, 523, 357
- Najarro, F., Hillier, D. J., & Stahl, O. 1997, *A&A*, 326, 1117
- Nielsen, K. E., Corcoran, M. F., Gull T. R., Hillier, D. J., Hamaguchi, K., Ivarsson, S. & Lindler, D. J. 2007, ([astro-ph/0701632](https://arxiv.org/abs/astro-ph/0701632))
- Pittard, J. M., & Corcoran, M. F 2002, *A&A*, 383, 636
- Pittard, J. M., & Dougherty, S. M. 2006, *MNRAS*, 372, 801
- Pittard, J. M., Stevens, I. R., Corcoran, M. F., & Ishibashi, K. 1998, *MNRAS*, 299, L5
- Repolust, T., Puls, J., & Herrero, A. 2004, *A&A*, 415, 349
- Ruffert, M. 1996, *A&A*, 311, 817
- Ruffert, M. 1999, *A&A*, 346, 861
- Schaerer, D. & de Koter, A. 1997, *A&A* 322, 598
- Smith, N., Davidson, K., Gull, T.R., Ishibashi, K., & Hillier, D.J. 2003, *ApJ*, 586, 432
- Smith, N., Morse, J. A., Collins, N. R., & Gull, T. R. 2004, *ApJ*, 610, L105
- Soker, N. 2001, *MNRAS*, 325, 584
- Soker, N. 2003, *ApJ*, 597, 513
- Soker, N. 2004, *ApJ*, 612, 1060

- Soker, N. 2005a, ApJ, 619, 1064
- Soker, N. 2005b, ApJ, 635, 540
- Soker, N. 2007, ApJ, (astro-ph/0610655)
- Soker, N. & Behar, E. 2006, ApJ, in press (astro-ph/0605723)
- Stahl, O., Weis, K., Bomans, D. J., Davidson, K., Gull, T. R. & Humphreys, R. M. 2005, A&A, 435, 303
- Steiner, J. E., & Damineli, A. 2004, ApJ, 612, L133 (SD04)
- van Genderen, A. M., de Groot, M. J. H., & The, P. S. 1994, A&A, 283, 89
- van Genderen, A. M., Sterken, C., de Groot, A., & Burki, G. 1999 A&A, 343, 847
- Verner, E., Bruhweiler, F. & Gull, T. 2005, ApJ, 624, 973
- Weis, K., Stahl, O., Bomans, D. J., Davidson, K., Gull, T. R., & Humphreys, R. M. 2005, AJ, 129, 1694
- Whitelock, P. A., Feast, M. W., Marang, F., & Breedt, E. 2004, MNRAS, 352, 447
- Zanella, R., Wolf, B., & Stahl, O. 1984, A&A, 137, 79